

Dynamics of cerebral blood flow regulation explained using a lumped parameter model

METTE S. OLUFSEN,¹ ALI NADIM,² AND LEWIS A. LIPSITZ³

¹Department of Mathematics, North Carolina State University, Raleigh, North Carolina 27695;

²Keck Graduate Institute, Claremont Graduate University, Claremont, California 91711;

and ³Hebrew Rehabilitation Center for Aged, Beth Israel Deaconess Medical Center, and Harvard Medical School, Boston, Massachusetts 02131

Received 22 May 2001; accepted in final form 10 October 2001

Olufsen, Mette S., Ali Nadim, and Lewis A. Lipsitz. Dynamics of cerebral blood flow regulation explained using a lumped parameter model. *Am J Physiol Regulatory Integrative Comp Physiol* 282: R611–R622, 2002; 10.1152/ajpregu.00285.2001.—The dynamic cerebral blood flow response to sudden hypotension during posture change is poorly understood. To better understand the cardiovascular response to hypotension, we used a windkessel model with two resistors and a capacitor to reproduce beat-to-beat changes in middle cerebral artery blood flow velocity (transcranial Doppler measurements) in response to arterial pressure changes measured in the finger (Finapres). The resistors represent lumped systemic and peripheral resistances in the cerebral vasculature, whereas the capacitor represents a lumped systemic compliance. Ten healthy young subjects were studied during posture change from sitting to standing. Dynamic variations of the peripheral and systemic resistances were extracted from the data on a beat-to-beat basis. The model shows an initial increase, followed approximately 10 s later by a decline in cerebrovascular resistance. The model also suggests that the initial increase in cerebrovascular resistance can explain the widening of the cerebral blood flow pulse observed in young subjects. This biphasic change in cerebrovascular resistance is consistent with an initial vasoconstriction, followed by cerebral autoregulatory vasodilation.

cerebral autoregulation; arterial modeling

THE DYNAMIC CEREBRAL BLOOD FLOW RESPONSE to sudden hypotension during posture change is poorly understood. The aim of this work is to use a lumped parameter model of cerebral blood flow to analyze changes in key parameters (systemic and peripheral cerebrovascular resistances) during posture change from sitting to standing. Such a model sheds light on vascular adaptation to hypotensive stress and could ultimately help determine the changes in cerebral autoregulation that occur in aging, hypertension, and other clinical conditions.

The present work focuses on the middle cerebral artery (MCA) and its peripheral vascular bed. The MCA is considered a conduit vessel, and the smaller

arteries and arterioles that branch off from the MCA are modeled as resistance vessels that dilate or constrict to restore blood flow when the perfusion pressure decreases or increases, respectively. The cerebral autoregulatory response to pressure reduction during posture change from sitting to standing is vasodilation of the arterioles. However, the dynamic cerebral blood flow response to posture change reflects not only the relative contributions from the peripheral cerebrovascular resistance, but also changes in systemic resistance, compliance, and heart rate.

To understand the regulatory response, transcranial Doppler (TCD) measurements of cerebral blood flow velocity in the MCA and Finapres measurements of arterial pressure in the finger from 10 healthy young subjects were analyzed using a three-element windkessel model. Blood flow in the MCA was obtained by multiplying the blood flow velocity by the area of the MCA (assumed constant throughout the study). As shown in Fig. 1, when the subject stands up (after 60 s of sitting) the pressure falls and the blood flow pulse widens (systolic minus diastolic value is increased). After subject stands for 20 s (i.e., 80 s into the study), both arterial pressure and flow reach a new “steady” state.

The three-element windkessel model is comprised of two resistors and a capacitor (see Fig. 2). We hypothesize that the windkessel model represents the MCA as a constant-diameter conduit vessel attached to a branching arbor of vessels representing the cerebrovascular bed. The capacitor and one of the resistors are considered lumped parameters, representing the vessels leading to (and including) the MCA, whereas the other resistor represents the resistance of the peripheral cerebrovascular bed.

We present an analysis that demonstrates that by allowing the windkessel model parameters to vary in time, one can successfully relate the pressure measured in the finger to the blood flow velocity measured in the MCA. Our model shows that the cerebrovascular resistance initially increases, possibly due to barore-

Address for reprint requests and other correspondence: M. S. Olufsen, Dept. of Mathematics, North Carolina State University, Box 8205, Raleigh, NC 27695 (E-mail:msolufse@unity.ncsu.edu).

The costs of publication of this article were defrayed in part by the payment of page charges. The article must therefore be hereby marked “advertisement” in accordance with 18 U.S.C. Section 1734 solely to indicate this fact.

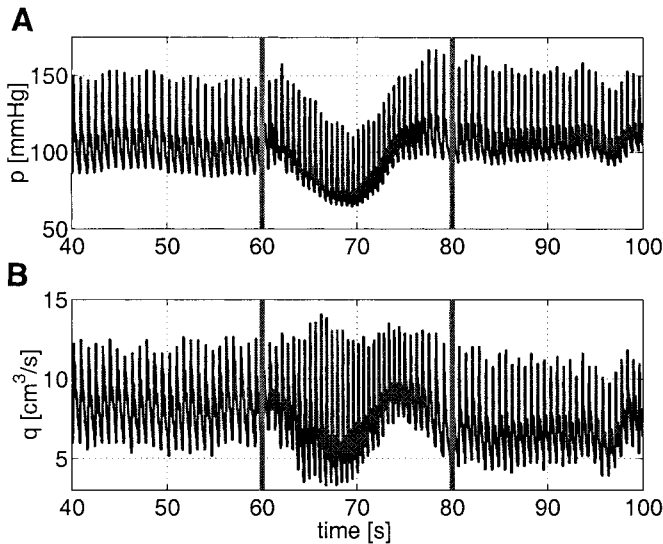


Fig. 1. Measured arterial pressure p (A) and flow q (B) during posture change. Immediately after standing (marked with vertical lines at $t = 60$ s) the pressure drops while the flow pulsatility widens (systolic minus diastolic flow increases). After standing for 20 s (at $t \approx 80$ s, marked with another set of vertical lines) the flow and pressure return to new steady state values.

flex-mediated regulatory responses to falling pressure, before the cerebral autoregulatory response sets in to dilate the vessels and decrease the cerebrovascular resistance. In addition, our work indicates that the initial increase in cerebrovascular resistance is responsible for the widening of the blood flow pulse.

We have chosen to work with the simple three-element windkessel model, because one aim of this work is to demonstrate a new methodology for data analysis rather than to develop a complex lumped model that can capture all details of the individual pulse profiles. Even with this simple model, we were able to reproduce dynamic changes in the pulsatile blood flow of the MCA during transient changes in arterial pressure.

METHODS

Modeling. The model used in this work is a three-element windkessel model often used in cardiovascular studies (27, 35, 48). The windkessel model can be represented by a circuit consisting of two resistors R_S and R_P (mmHg · s/cm³) and a capacitor C_S (cm³/mmHg) (see Fig. 2). We assume that C_S and R_S represent the systemic compliance and resistance of the arteries leading to (and including) the MCA, whereas R_P represents the resistance associated with the peripheral cerebrovascular bed. Because it is difficult to make measurements of pressure directly in the MCA the input to the model is pressure in the finger (p_F , mmHg; alternatively one could use pressure measurements from the earlobe). The output from the model is the volumetric flow rate (q_{MCA} , cm³/s) in the MCA, which can be validated by comparison with corresponding measured data. In addition to the above elements, the circuit includes intermediate flow and pressures: the flow and pressure of the peripheral cerebrovascular bed (q_P , p_P) the venous pressure (p_V), and the intracranial pressure (p_I). However, these will not be determined explicitly. If we assume that flow and pressure are correlated (20) we can use an electrical circuit analogy and

derive equations for pressure and flow in the MCA. Assuming that the pressure and flow can be described as sums of harmonic components of the form $p(t) = Pe^{i\omega t}$ and $q(t) = Qe^{i\omega t}$ where ω (s⁻¹) is frequency, t (s) is time, and P , Q are pressure and flow in the frequency domain. Using these definitions, the equations for the circuit in Fig. 2 are

$$P_F - P_P = R_S Q_{MCA}$$

$$P_P - P_V = R_P Q_P$$

$$P_P - P_I = \frac{Q_{MCA} - Q_P}{i\omega C_S}$$

Assuming that $P_V = P_I = 0$ the above equations yield

$$\frac{P_F}{Q_{MCA}} = \frac{R_P + R_S + i\omega C_S R_S R_P}{1 + i\omega C_S R_P} \equiv Z_W(\omega) \tag{1}$$

where, as is common for electrical circuits, the impedance is defined as $Z = P/Q$ (mmHg · s/cm³).

More generally, for time-periodic signals of period T (s) (the length of the cardiac cycle), the theory of Fourier series gives

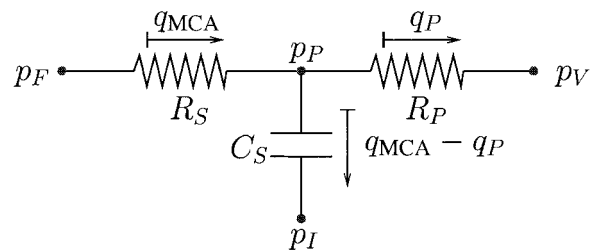
$$p(t) = \sum_{k=-\infty}^{\infty} P(\omega_k) e^{i\omega_k t}, \quad q(t) = \sum_{k=-\infty}^{\infty} Q(\omega_k) e^{i\omega_k t}$$

with

$$P(\omega_k) = \frac{1}{T} \int_{-T/2}^{T/2} p(t) e^{-i\omega_k t} dt, \quad Q(\omega_k) = \frac{1}{T} \int_{-T/2}^{T/2} q(t) e^{-i\omega_k t} dt$$

where $\omega_k = 2\pi k/T$ and $-T/2 \leq t \leq T/2$, with the relation in Eq. 1 valid for each of the frequency components in the signal.

Using the above relationship between flow and pressure in the frequency domain, the windkessel Eq. 1 can also be written as the following ordinary differential equation in the time domain



- pressure (p) mmHg •
- flow (q) cm³/s →
- resistance (R) mmHg s/cm ⏏
- capacitance (C) cm³/mmHg ⏏
- (capacitance = compliance)

Fig. 2. The circuit representing the middle cerebral artery (MCA) and its peripheral cerebrovascular bed (subscript P). The capacitor C_S and resistor R_S are lumped parameters including the MCA and systemic arteries leading to the MCA. We assume that the pressure of the finger p_F is approximately the same as the pressure into the MCA. Finally, p_V is the pressure of the venous bed and p_I is the intracranial pressure.

$$R_S \left[\frac{dq_{MCA}}{dt} + \frac{(R_S + R_P)q_{MCA}}{C_S R_S R_P} \right] = \frac{dp_F}{dt} + \frac{p_F}{C_S R_P} \quad (2)$$

Note that the combination of parameters $C_S R_P$ and $C_S R_S R_P / (R_S + R_P)$, which appear as coefficients on the two sides of Eq. 2, can be regarded as the characteristic relaxation times in this model. Furthermore, if pressure $p(t)$ is regarded as input, this equation can be integrated to find $q(t)$ provided that the parameters are known.

The above interpretation of the lumped model is based on the location of the blood flow velocity measurements. Effects due to changes in venous and intracranial pressure are not specifically included in the model. However, even though the model is simple, it is still able to capture dynamic effects arising due to posture change. Another important factor is that having a simple model with a small number of parameters makes it easy to extract the dynamic variation of each of the parameters from the measured data.

As mentioned earlier, the measurements provide data for pressure in the finger and for velocities in the MCA. The windkessel model provides a relation between blood flow (volumetric flow rate) and pressure, not velocity and pressure. To obtain values for the flow, we assume that the MCA has a constant radius of $r = 2$ mm and the flow is $q = \pi r^2 v$ (cm³/s), where v (cm/s) is the blood flow velocity. The radius of the MCA varies among the different subjects; however, because direct measurements of the radius are not available, we simply assume it to be constant. All data shown in the results section are based on the flow q (rather than the velocity).

Let Z_W be the impedance obtained from the windkessel model (Eq. 1) and let Z_m be the impedance obtained from the measurements by taking the ratio of the discrete Fourier transform of the pressure and flow data. Then, the parameters for the windkessel model can be determined by fitting the impedance of the windkessel model to the impedance of the data.

The zero- and large-frequency limits of the windkessel model (Eq. 1) yield relations that only involve the resistances

$$\lim_{\omega \rightarrow \infty} Z_W(\omega) = R_S, \quad \lim_{\omega \rightarrow 0} Z_W(\omega) = R_S + R_P \quad (3)$$

For the measured impedances, the limit $\omega \rightarrow 0$ corresponds to the direct current (DC) value of the impedance, and the limit $\omega \rightarrow \infty$ corresponds to the highest meaningful frequency in the measured data. The data contain a significant amount of noise and hence the high-frequency limit is better approximated by taking the mean value of the measured impedance over a number of high frequencies.

Once R_S and R_P have been determined, C_S can be computed from analyzing the modulus of the impedance $|Z|$ as a function of frequency. This can be done by estimating the measured impedance at a point where the impedance curve obtained by the windkessel model passes through the impedance obtained by the measured data (e.g., between the 2nd and 3rd data points in Fig. 3). The magnitude of the measured impedance at this point is

$$|\bar{Z}_m(\omega_{2,3})| = \frac{|Z_m(\omega_2)|}{2} + \frac{|Z_m(\omega_3)|}{2}$$

and the frequency at this point is

$$\omega_{2,3} = \frac{\omega_2}{2} + \frac{\omega_3}{2}$$

From (Eq. 1) we have

$$|Z_W|^2 = \frac{(R_P + R_S)^2 + (\omega C_S R_S R_P)^2}{1 + (\omega C_S R_P)^2}$$

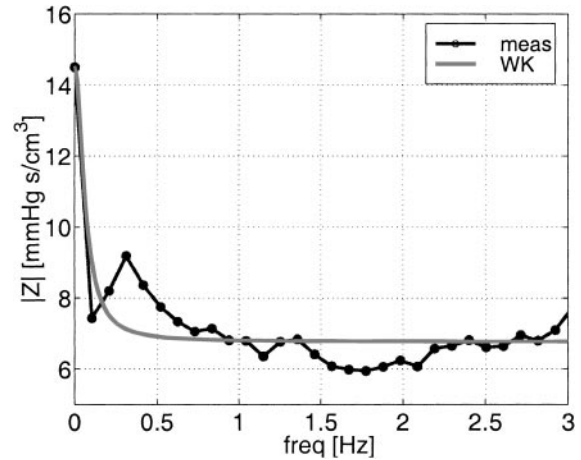


Fig. 3. Modulus of the impedance $|Z(\omega)|$ obtained using a windowed Fourier transform of the data. The window was a box window with 50% overlap and length 480. The solid black line with dots represents the measured data, and the gray line represents the results obtained using the windkessel model.

Inserting the averaged values for $\omega_{2,3}$ and $\bar{Z}(\omega_{2,3})$ and solving for C_S yields

$$C_S = \sqrt{\frac{(R_S + R_P)^2 - |\bar{Z}(\omega_{2,3})|^2}{\omega_{2,3}^2 R_P^2 (|\bar{Z}(\omega_{2,3})|^2 - R_S^2)}} \quad (4)$$

We have estimated the parameters of the windkessel model by analyzing the data in two ways. First, we estimated parameters representing three periods: sitting (0–60 s), transition from sitting to standing (60–80 s), and standing (80–120 s). This was done by means of the windowed Fourier transform. Second, we estimated the parameters on a beat-to-beat basis, thus enabling us to monitor how they change during posture change, and hence, how autoregulation affects the peripheral cerebrovascular bed.

The windowed Fourier transform (WFT) or the sliding Fourier transform is widely used for extracting time-dependent spectra from a finite length time series. It divides the time series into a finite number of smaller series, which is individually Fourier transformed. Each section is analyzed for its frequency content and then averaged over the finite number of sections. The advantage of this technique is that significant frequencies do not vanish, as would often occur if the full sequence were analyzed using a conventional Fourier transform (FFT) method. Because a single window is used for all frequencies in the WFT, the resolution of the analysis is the same (equally spaced) at all locations in the time-frequency domain.

FFT works well for signals with smooth or uniform frequencies, but it has been found that the windowed Fourier transform works better with signals having pulse-type characteristics, time-varying (nonstationary) frequencies, or odd shapes. The FFT does not distinguish sequence or timing information. For example, if a signal has two frequencies (a high followed by a low or vice versa), the Fourier transform only reveals the frequencies and relative amplitude, not the order in which they occurred. So Fourier analysis works well with stationary, continuous, periodic, differentiable signals, but other methods such as the WFT are needed to deal with nonperiodic or nonstationary signals.

Figure 3 shows a comparison of the impedances from the data and the windkessel model during the sitting period for a window size of 480. The data were sampled at 50 Hz; hence,

a window containing 480 data points covers 9.6 s. Thus, the data points in Fig. 3 are in frequency increments of $1/9.6 = 0.104$ Hz. The window type that gave the most consistent results was a box window with a 50% overlap. This analysis was carried out using a function from Matlab's signal processing toolbox (21). The zero-frequency limit $Z_m(0) = R_S + R_P$ of the WFT data can be obtained directly by picking out the DC value of Z_m . However, for high frequencies the data are noisy so it is more difficult to find R_S . We investigated several options and found the most stable results when R_S is chosen as the mean over frequencies < 8 Hz (or an angular frequency < 40 radians/s). After the resistances have been estimated, C_S was obtained using Eq. 4. It may be noted that the drop of $|Z|$ occurs over the first few points that have frequencies of order 0.1 Hz or periods of order 10 s. Thus, when we analyze the data on a beat-to-beat basis, there is not enough resolution in the frequency intervals to estimate the compliance.

The same criteria were used when the parameters were determined on a beat-to-beat basis. However, to find the parameters on a beat-to-beat basis, the time series must be separated at the beginning of each cardiac cycle. This can be done by searching the pressure data for local minima. Each period will have two minima: one representing the beginning of a cardiac cycle and the other representing the beginning of the diastolic notch (see Fig. 4). The stars in Fig. 4 represent the beginning of the cardiac cycle. A similar analysis cannot be performed using the blood flow velocity data, because the levels of noise are significantly higher and as a result there will be a large number of local minima. Because pressures and flows are recorded simultaneously, knowing the length of the cardiac cycle and the local minima for the pressure enables us to find the local minima for the flow. The only difference is that there could be a small phase lag between the flow and pressure minima because the data were not measured at the same location.

The impedances can be found using the same method as for the WFT. The only difference is that instead of calculating Z_m over the full interval (sitting, transition, or standing) it was calculated for each cardiac cycle. However, as discussed above, the C_S cannot be calculated on a beat-by-beat basis because the main variation in the impedance occurs at very low frequencies (corresponding to periods that are longer than a single cardiac cycle). This can be seen from Fig. 5: the impedance curve obtained by the windkessel model is already flat when the first data point has reached the level of R_S . The measured data are acquired at 50 Hz, so for a cardiac cycle of 1.2 s we get 60 data points with a difference between discrete frequencies of $1/1.2 = 0.83$ Hz. For the WFT, the interval with a window size of 480 data points comprises approximately eight cardiac cycles or $8 \times 1.2 = 9.6$ s. The interval between two discrete frequencies is 0.1 Hz. So to calculate the compliance from the data only one mean value can be obtained for each of the three states: sitting, transition, and standing.

Comparing R_S and R_P obtained by the WFT during sitting with the average of those obtained on a beat-to-beat basis, the results are consistent (see Fig. 5C). Similar results can be obtained during the period of standing. However, during the transitional period from sitting to standing, the values obtained on a beat-to-beat basis vary significantly from the average values obtained from the windowed Fourier transform.

In addition to the resistances and the compliance, the heart rate also varies on a beat-by-beat basis. By separating the time series at the beginning of each cardiac cycle, the

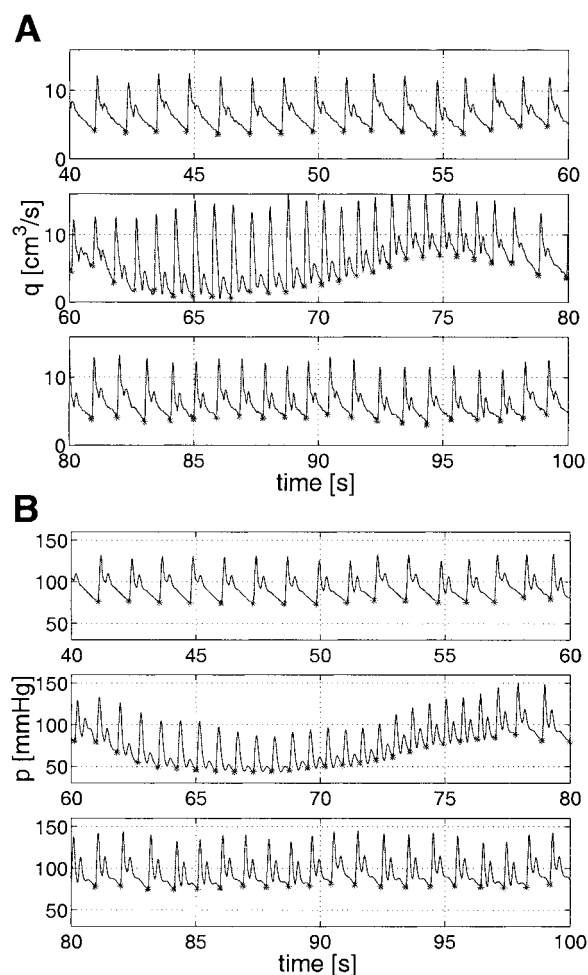


Fig. 4. Consecutive flow q (A) and pressure p (B) profiles for each cardiac cycle during a 100-s trial in 1 subject. Each cardiac cycle has 2 minima, 1 at the beginning of the cardiac cycle (*) and one at the diastolic notch. Note, the blood flow velocity and pressure are measured at 2 different locations and due to differences in the distance, the pulse wave will not reach the 2 locations at the same time. Hence, there is a constant phase lag (6 ms for this subject) between the 2 sites. This has been corrected for in the graphs.

heart rate is simply obtained by $HR = 1/T$ (beats/min) where T is the duration of the cardiac cycle.

Assuming that pressure is known (see Fig. 1) and that the parameters in the windkessel model have been determined as describe above, the flow can be computed by integrating the differential Eq. 2 and comparing the results with the measured values (see Fig. 9). Simulations were carried out for ten healthy young subjects. The computed pulsatile flow profiles were compared with the actual transcranial Doppler measurements. Comparisons were made both with respect to quantitative agreement over the entire dynamic range as well as with mean flow, and systolic and diastolic flows for the two steady-state situations (before and after standing). Statistical significance was determined using two-way analysis of variance (22) and P values < 0.05 were considered statistically significant.

Experimental methods. The subjects of this study are ten carefully screened healthy young volunteers aged 20–39 years, whose mean cerebral autoregulatory responses to posture change and carbon dioxide are described elsewhere (20).

During the protocol, heart rate was measured continuously from a three-lead electrocardiogram, and beat-to-beat

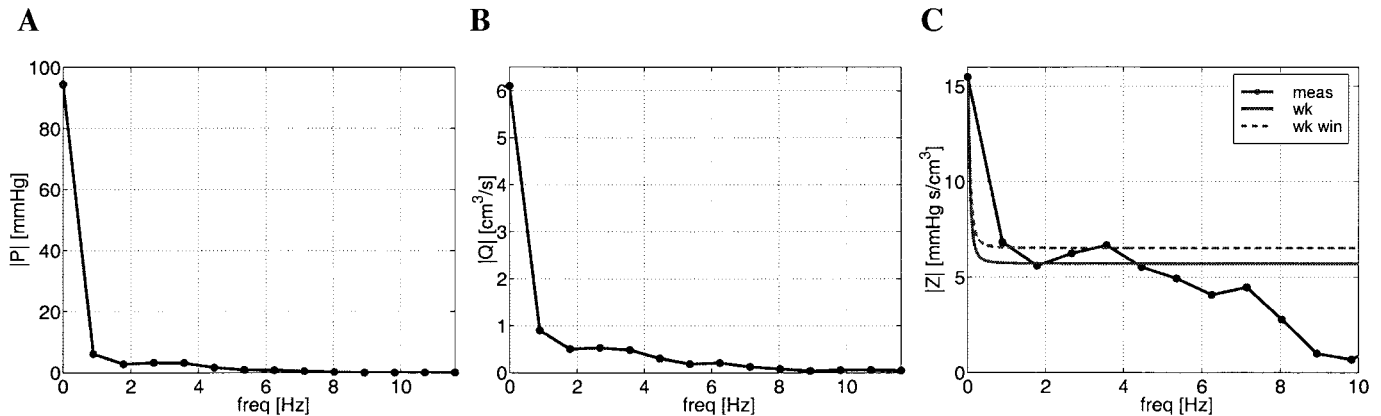


Fig. 5. Fourier transforms of pressure $P(\omega)$ (A), flow $Q(\omega)$ (B), and their ratio (impedance) (C). The graphs show the absolute value as a function of frequency using a single period during sitting (the period starting at 29.12 s). In C, the impedance obtained from the data (solid line with circles) is compared with that obtained by the windkessel model (solid line) and the windowed Fourier transform (dashed line). Note, the compliance cannot be found from the Fourier transform of a single period because the frequency resolution is too low. Thus the value of C_S used is based on the windowed Fourier transform shown in Fig. 3.

arterial pressure was determined noninvasively from the middle finger of the nondominant hand using a photoplethysmographic noninvasive pressure monitor (Finapres) supported by a sling at the level of the right atrium to eliminate hydrostatic pressure effects. To keep end-tidal CO_2 constant, respiration was measured continuously using an inductive plethysmograph (Respirace) and subjects breathed at 0.25 Hz (15 breaths/min) throughout each standing procedure by following tape-recorded cues. All subjects underwent Doppler ultrasonography by a trained technician to measure the changes in blood flow velocity within the MCA in response to active standing. The 2-MHz probe of a Nicolet Companion portable Doppler system was strapped over the temporal bone and locked in position with a Mueller-Moll probe fixation device to image the MCA. The MCA blood flow velocity was identified according to the criteria of Aaslid (1) and recorded at a depth of 50–65 mm. The envelope of the blood flow velocity waveform, derived from a Fast-Fourier analysis of the Doppler frequency signal, and continuous pressure and electrocardiogram signals were digitized at 250 Hz and stored in the computer for later offline analysis.

After instrumentation, subjects sat in a straight-backed chair with their legs elevated at 90 degrees in front of them on a stool. For each of two active stands, subjects rested in the sitting position for 5 min then stood upright for 1 min. The initiation of standing was timed from the moment both feet touched the floor. Data were collected continuously dur-

ing the final minute of sitting and the first minute of standing during both trials.

The study was approved by the Institutional Review Board at the Hebrew Rehabilitation Center for Aged and all subjects provided written informed consent.

RESULTS

Figure 1 shows the measured pressure and MCA blood flow during the transition from sitting to standing for one subject. While the pressure and flow levels vary among the subjects, the characteristics of the profiles are similar for all subjects. Immediately after the subjects stood up their pressure dropped and flow pulse widened. Approximately 10 s after standing (at $t \approx 70$ s) the pressure started to increase and the flow pulse narrowed, reaching a new steady state at $t \approx 80$ s.

Table 1 shows mean values \pm SD for blood flow and pressure during sitting, transition, and standing. There was no statistically significant difference between sitting and standing values for pressure although the flows were significantly decreased during standing. During the transition there were statistically significant changes in both pressure and flow. The

Table 1. Mean, systolic, and diastolic arterial pressures p and flows q , and heart rate (beats/min) during sitting (0–60 s), transition (60–80 s), and standing (80–120 s)

Parameter	Unit	Sitting	Transition	P Value Sit-Trans	Standing	P Value Sit-Stand
Mean p	mmHg	94.20 \pm 8.93	68.02 \pm 11.17	0.000	94.32 \pm 9.95	0.933
Systolic p	mmHg	134.97 \pm 13.60	103.61 \pm 20.18	0.000	136.22 \pm 17.30	0.557
Diastolic p	mmHg	75.46 \pm 8.55	54.20 \pm 9.34	0.000	77.84 \pm 9.68	0.053
Mean q	cm ³ /s	6.39 \pm 1.11	8.55 \pm 1.40	0.000	5.80 \pm 1.21	0.000
Systolic q	cm ³ /s	10.54 \pm 1.94	13.02 \pm 2.54	0.000	10.00 \pm 2.10	0.002
Diastolic q	cm ³ /s	4.35 \pm 0.83	6.81 \pm 1.17	0.000	4.11 \pm 0.93	0.026
Heart rate	beats/min	70.56 \pm 13.96	67.70 \pm 11.62	0.043	76.39 \pm 14.91	0.000

All data represent an average \pm SD for all 10 subjects. The P values compare the results to the sitting values using a two-way analysis of variance.

mean, systolic, and diastolic pressures and the mean and diastolic flows decrease, whereas the systolic flow increases. The heart rate increases during standing and remains slightly increased until the end of the study.

Using the measured pressure and flow, we were able to extract the dynamic changes of the windkessel model parameters during posture change. These parameter changes are shown for one subject in Fig. 6. The results show that during posture change, the mean flow and pressure decrease for about 10 s and then increase for about 10 s, while the ratio of pressure to flow (the total resistance $R_P + R_S$) increases slightly, then falls for about 10 s, and then increases for about 10 s to a new steady state. The peripheral cerebrovascular resistance R_P increases significantly (for a few seconds) in the beginning before it falls. As expected, the heart rate increases for 10–15 s, and then it falls to the new steady state.

The total resistance is the most one can determine by simply studying the measured data. However, as shown in Fig. 6, we have been able to obtain more

information using the windkessel model by decomposing the resistance into a systemic and a peripheral (cerebrovascular) part. Figures 6, and 8–11 all contain data for one subject; but, data for the other subjects are very similar. The results for the entire study cohort are summarized in Table 2 and Fig. 7. The table shows that the changes in resistances and compliance are all statistically significant. However, as shown in Fig. 7, interindividual variation is fairly large. During sitting and standing, the standard deviation is 30%, while during the transition it is nearly 40%. Comparisons of the two trials within subjects shows good intraindividual reproducibility for most subjects.

As shown in Fig. 8 the compliance has not been analyzed on a beat-to-beat basis. Steady-state compliance values were obtained during each of the three periods: sitting, transition, and standing. To illustrate the change in compliance, we have interpolated linearly between the two steady states and the transition state. The compliance decreases and then increases to a new steady state that is slightly lower than its original value.

Fig. 6. The traces (top to bottom) show pressure p (mmHg) (A), flow q (cm^3/s) (B), mean pressure (p mean) (mmHg) (C), mean flow (q mean) (cm^3/s) (D), total resistance (p mean/ q mean) or $R_P + R_S$ (mmHg s/ cm^3) (E), systemic resistance (including the MCA) R_S (mmHg s/ cm^3) (F), peripheral cerebrovascular resistance R_P (mmHg s/ cm^3) (G), and heart rate (beats/s) (H) all as functions of time (s).

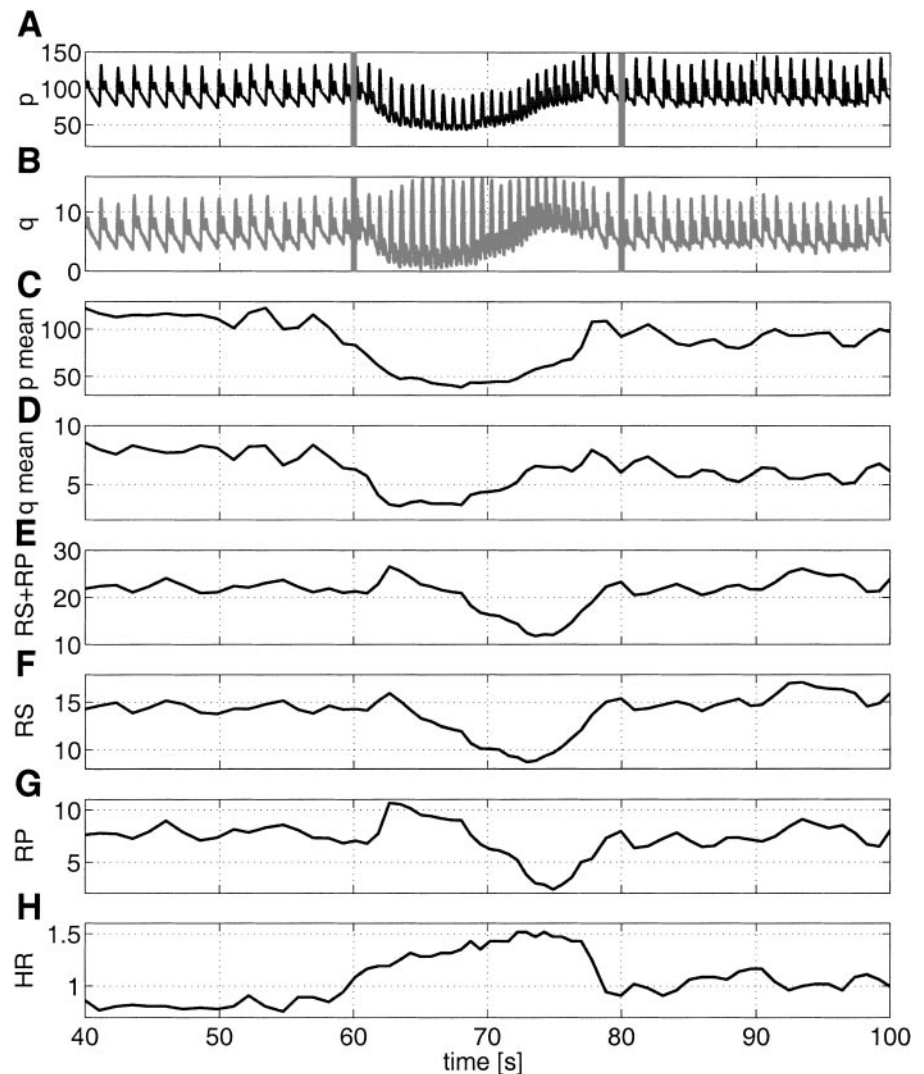


Table 2. Average values, standard deviation, and the *P* value (with a 5% significance level) for each of the parameters R_S , R_P , and $R_S + R_P$, and C_S for all 10 subjects

Param	Unit	Sitting	Min Trans		Max Trans		Standing	
		Mean	Mean	<i>P</i> Value Sit→Min Trans	Mean	<i>P</i> Value Sit→Max Trans	Mean	<i>P</i> Value Sit→Stand
R_S	mmHg s/cm ³	10.6 ± 2.9	5.7 ± 2.4	0.000			11.5 ± 3.9	0.026
R_P	mmHg s/cm ³	5.4 ± 2.2	3.4 ± 2.0	0.000	9.1 ± 2.4	0.000	6.7 ± 2.4	0.001
$R_S + R_P$	mmHg s/cm ³	16.0 ± 3.3	11.9 ± 2.6	0.000			18.2 ± 4.5	0.000
C_S	cm ³ /mmHg	3.3 ± 1.5	0.9 ± 0.5	0.000			2.7 ± 1.0	0.003

Note, for each subject the values for sitting (0–60 s) and standing (80–120 s) are obtained by averaging over the periods, while for the transition (60–80 s) the minimum and maximum values are shown. The *P* values compare the results to the sitting values using a two-way analysis of variance.

Figure 9 illustrates the result of applying the parameters obtained in Fig. 6 for the full duration of the measurements. The top trace shows the computed flow and the bottom trace shows the measured flow. The vertical lines at the 60-s mark where the subject stands up, and the vertical lines at 80-s mark approximately when flow and pressure have returned to the new steady state during standing. The figure shows a very good correspondence between the measured and computed flows. However, Fig. 9 does not show how well-computed and measured flows compare on a beat-to-beat basis. To make this comparison we have computed

beat-to-beat profiles at three different times, at approximately 17 s, 70 s, and 85 s. These traces shown in Fig. 10 exhibit good correspondence between the measured and the computed data. Both the profiles in Fig. 10 and the impedance plots in Figs. 3 and 5 show some extra “bumps” that are not captured by the model. In Fig. 10, the bumps appear immediately before the reflected wave. In the impedance curves in Fig. 3, the extra bump occurs just after the initial drop from the DC value. These bumps could be due to the presence of inertia which is not included in the model. Lumped models studied by Toy et al. (38) have shown that

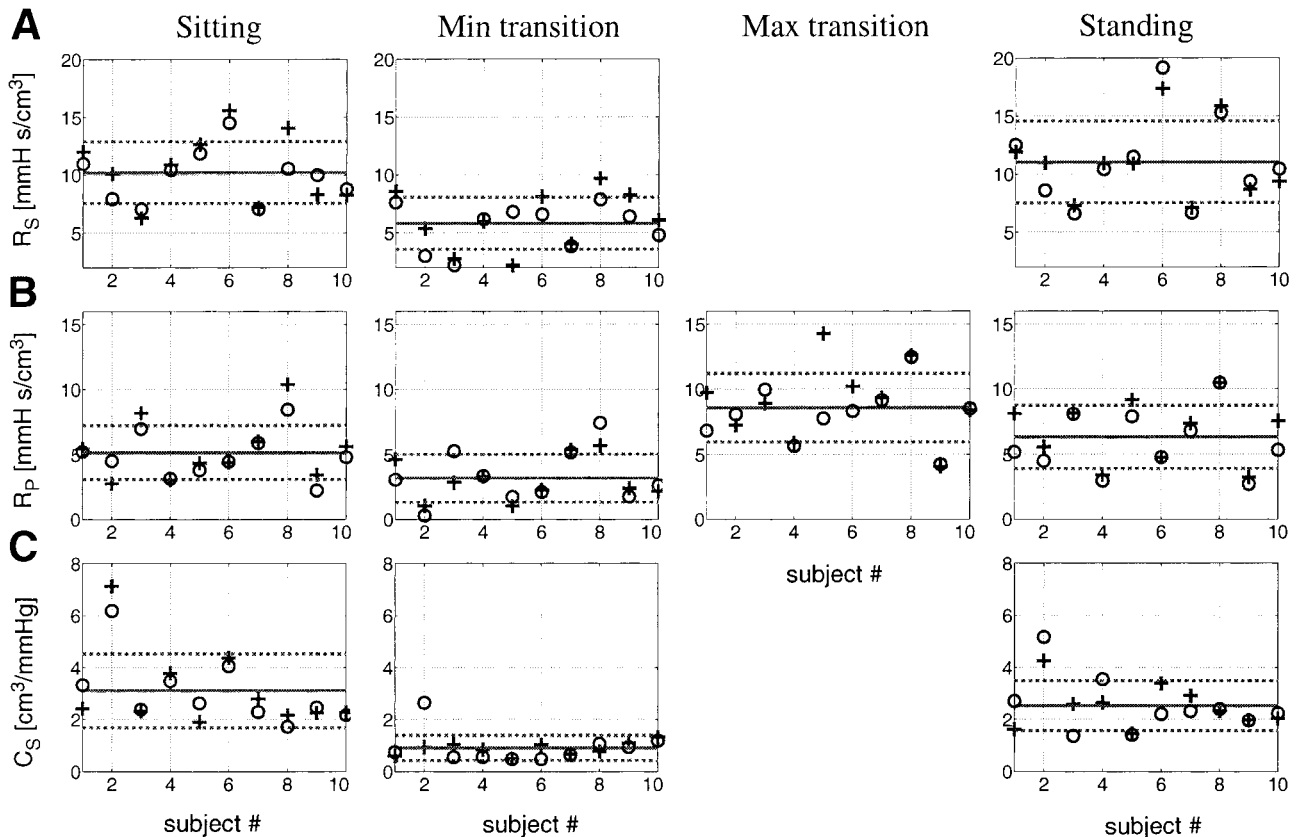


Fig. 7. Average values for the parameters R_S (A), R_P (B), and C_S (C) during each of the 3 periods. The averages for the resistances are found by averaging the data obtained on a beat-to-beat basis for 2 trials for each subject. The horizontal axis plots each subject (circles are used for *trial 1* and plusses for *trial 2*). The vertical axis shows the average resistances or compliance. The solid line represents the mean over all subjects and the dotted lines the standard deviation.

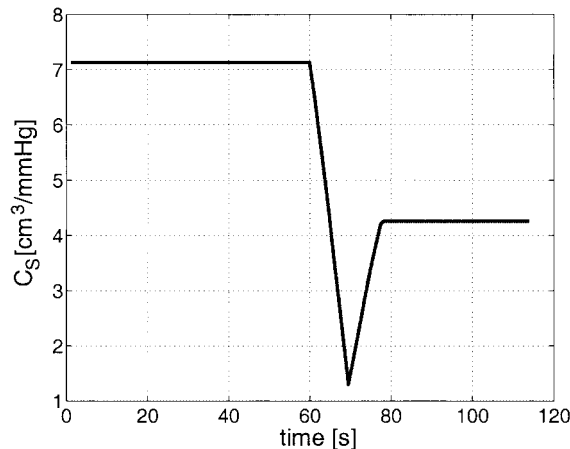


Fig. 8. The compliance C_S is based on the values obtained using window-based Fourier analysis. Hence, each of the 3 periods is represented by an average compliance. Linear interpolation is used to account for variation of compliance during the transition period.

features similar to the ones seen in our data can be captured by including more elements (e.g., inertances or more resistors and capacitors) into the model.

DISCUSSION

Blood flow in the cerebral circulation is controlled by a dynamic regulatory system. The regulation is active over a range of time scales lasting from a few seconds to several minutes. The purpose of control is to maintain a constant flow over a wide range of pressures. This is done by regulating the diameters of vessels in the peripheral cerebrovascular bed as well as by changing the heart rate and cardiac output. The control appears to be active within upper and lower limits of pressure (e.g., in young subjects, 50–150 mmHg) that shift toward higher pressures in hypertensive subjects (36). The autoregulatory control process in the cerebral vasculature is most likely mediated by a combination of myogenic and metabolic mechanisms, as well as changes in the activity of the autonomic nervous system (29), but it is not yet fully understood. This paper focuses on modeling the dynamics and control of cerebral blood flow with the goal of better understanding the regulatory mechanisms in young adults. The three-element windkessel model used in this work included only very basic mechanisms, but we have shown that it is still able to reproduce the measured data. We have kept the model simple, because as discussed previously, we were interested in tracking how the windkessel parameters changed during posture change. Including more elements, and hence more parameters, would have made it much more difficult to develop a procedure for automatically monitoring the change of the parameters such that they could still be understood from basic principles.

There are several published models of cerebral autoregulation, but to our knowledge there are currently no other models that include both cerebral autoregulation and pulsatility. Pulsatile models have been developed for studying atherosclerosis in the carotid (30, 47) or

for studying the dynamics of blood flow in the circle of Willis (15, 17, 46). The models by Viedma et al. (46) and Kufahl and Clark (17) are distributed, i.e., they include time and one spatial dimension, whereas the model by Hillen (15) is based on lumped parameters. The models were developed to study the large anatomical variation of the communicating arteries and the effect of various pathological situations. The latter were verified by variation of the model parameters to represent alterations in flow distribution due to occlusions. Work by Ursino (42, 45) discusses the importance of pulsatility in carotid baroreflex regulation. Modeling pulsatility is important when studying perturbations such as mild hemorrhage, carotid occlusion maneuvers, or genesis of self-sustained arterial pressure waves.

Ursino and Lodi (39, 40, 42, 44) also made significant contributions to modeling cerebral blood flow velocity and its autoregulation. Their work is based on a steady-state model that mimics the behavior of the intracranial arterial vascular bed, intracranial venous vascular bed, cerebrospinal fluid absorption, and production. Model parameters were computed using physiological considerations and anatomical data from normal subjects. The cerebral circulation is represented by a steady-state lumped parameter model. Each of the elements in the model comprises a capacitor and a resistor, some of the capacitors being passive and some active. The elements represent the MCA, large and small pial arteries, the venous bed, the intracranial pressure, and the cerebrospinal fluid circulation. A regulation loop is applied at the large and small pial arteries. The large pial arteries respond actively to changes in cerebral perfusion pressure, whereas the small pial arteries are sensitive to percent changes in cerebral blood flow velocity. Dynamics of each mechanism are simulated by means of a gain factor and a first order low-pass filter with a time constant. Finally,

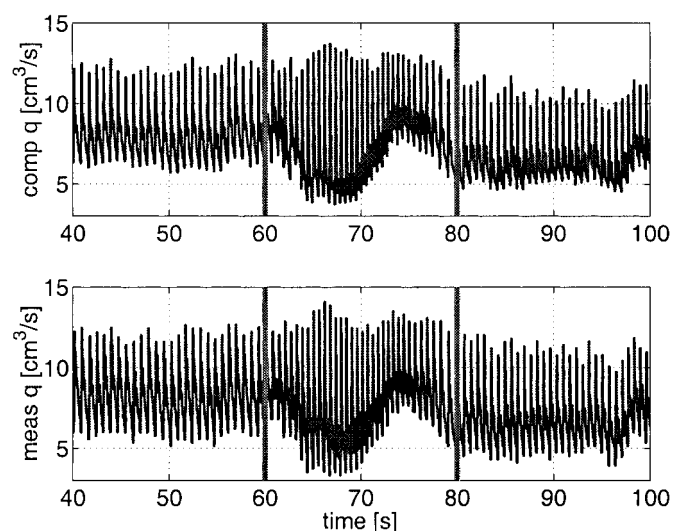


Fig. 9. Computed (*top trace*) and measured (*bottom trace*) flow q for the entire duration of the measurements. The vertical lines at the 60-s mark indicate where the subject stands up, and the vertical lines at the 80-s mark indicate where we estimate that the flow and pressure have returned to the new steady state during standing.

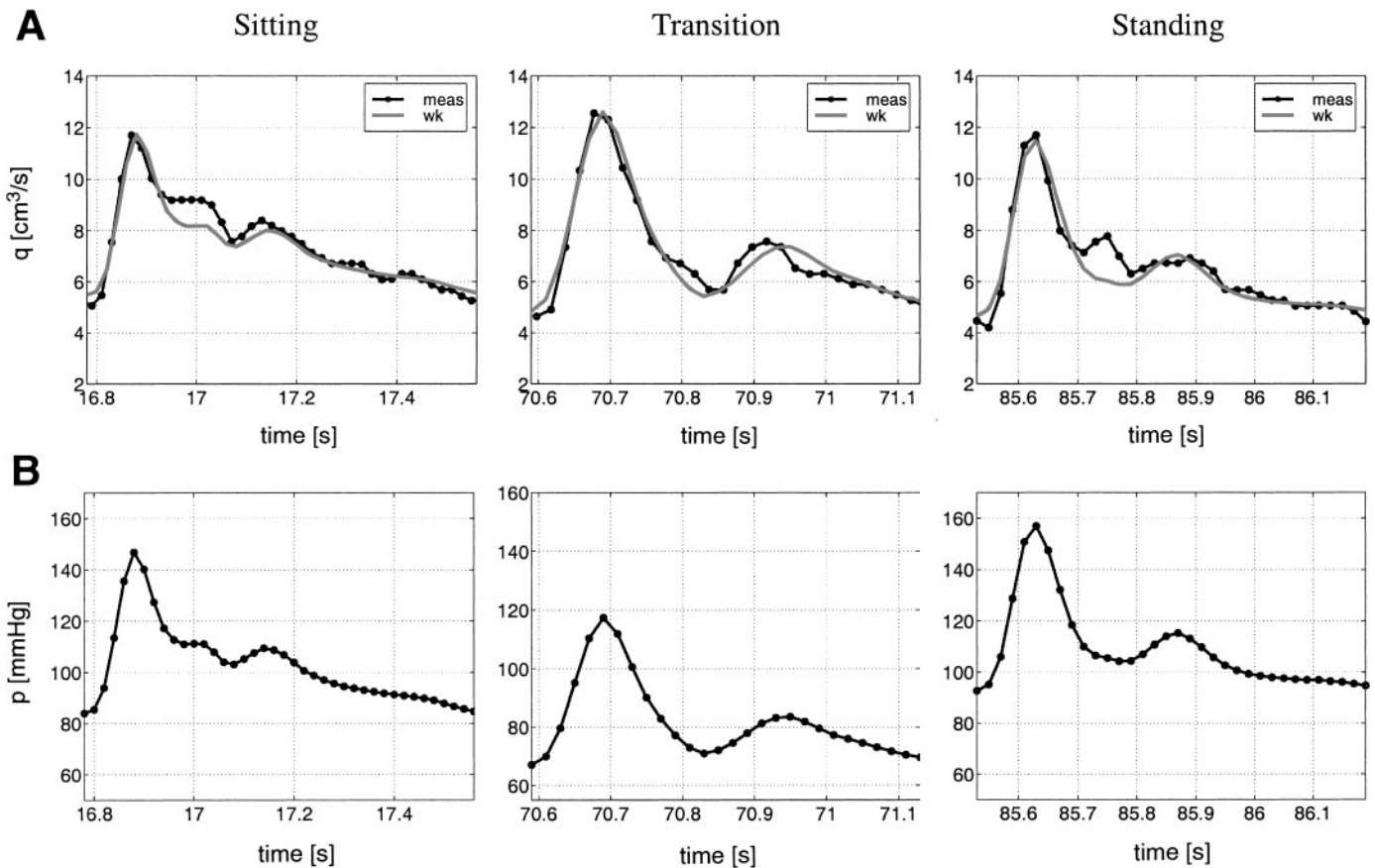


Fig. 10. Simultaneous recordings of blood flow q (A) in the MCA and arterial pressure p (B) in the finger (meas, solid line with filled circles) compared with computed MCA blood flow (wk, solid gray line) for 1 subject. The flow is obtained by multiplying the velocity with the constant cross-sectional area of the MCA (radius = 2 mm). The profiles are plotted during sitting (at $t \approx 17$ s), transition (at $t \approx 70$ s), and standing (at $t \approx 85$ s).

autoregulation interacts nonlinearly through a sigmoidal static relationship.

Ursino et al. (43) used the above model for studying effects of changes in intracranial pressure, systemic arterial pressure, autoregulation, and intracranial compliance using transcranial Doppler (TCD) waveforms (systolic, mean, and diastolic blood flow velocity, peak-to-peak amplitude, and pulsatility index). They concluded that information contained in the TCD waveform is affected by many factors, including intracranial pressure, systolic arterial pressure, and autoregulation. These factors can also be incorporated within the lumped parameter models which we have introduced here. Ursino and Gimmarco (41) studied the interaction of cerebral blood flow velocity and cerebral plateau waves, the effect of acute arterial hypotension on intracranial pressure, and the role of cerebral hemodynamics during pressure volume index tests. Recently, Ursino and Lodi (44) expanded the model to also account for CO_2 reactivity. To avoid the potential effect of changes in CO_2 , our study controlled breathing at 0.25 Hz and maintained a constant end-tidal CO_2 .

Other groups have also modeled the cerebral circulation, e.g., Gaffie et al. and Fincham and Tehrani (12, 13) who studied steady-state relationships between

cardiac output and cerebral blood flow velocity. This model described cerebral autoregulation in terms of arterial blood levels of oxygen and carbon dioxide and the metabolic rate ratio. Another example is a seven-compartment model developed by Bekker et al. (3), who investigated the effects of various vasodilatory/constrictive drugs on the intracranial pressure. The effects of drugs were modeled using a variable arteriolar-capillary resistance. Models reproducing pulsatile flow and pressure phenomena (2, 27, 28, 32, 35, 48) do not include dynamics of the regulation. These models were used to study dynamic changes in the flow and pressure as the pulse wave propagates along the arterial tree. All of the above models are distributed models (including one spatial dimension) determining flow and pressure at any given location of a vessel at all times. The models differ in the way they treat shear stresses, the relation between pressure and cross-sectional area, and the boundary conditions.

Our model is based on TCD methodology, which measures blood flow velocity in the MCA. Because blood flow through an artery can be estimated as the product of the true mean velocity and cross-sectional area, changes in velocity represent changes in cerebral volumetric flow, only if vessel diameter does not change. Several studies have validated TCD for the

measurement of cerebral blood flow velocity using both invasive and noninvasive methods. Newell et al. (25) compared changes in MCA velocities measured by TCD with invasive internal carotid blood flow measurements during rapid deflation of thigh blood pressure cuffs while subjects were undergoing carotid artery surgery. They found a strong linear correlation ($R = 0.995$). Other groups have also shown excellent correlations between TCD and invasive determinations of cerebral blood flow velocity in humans (18, 19). With the use of either the noninvasive xenon-133 method or single photon emission computerized tomography, flow velocities from the middle, anterior, and posterior cerebral arteries have been shown to correlate with simultaneously measured velocity values from corresponding cerebral regions (4, 5, 7, 34). The correlation coefficient is highest for the MCA (34), the vessel in which extensive data are available for this study. In humans it is likely that changes in velocity within the MCA correlate with changes in flow and constitute an acceptable index of flow in this arterial segment.

As described above our model assumes that the MCA does not change its diameter. This assumption is supported by several lines of evidence suggesting that the MCA diameter does not change during hypotensive stress induced by head-up tilt (6), lower body negative pressure (33), and a number of other stimuli (11, 13, 16, 18, 19, 25). Because our model has one resistive term (R_S) representing the systemic arterial circulation, which does change during the transition from sitting to standing (see Fig. 6), we assume that this change represents total systemic resistance rather than the resistance of the MCA. To address this question in more detail a more elaborate model is called for, where the MCA is modeled explicitly as a vessel with a given diameter.

As shown in the previous figures, we were able to obtain excellent agreement between the model and the measured results. Our results are consistent with the following physiological mechanism: immediately after standing up arterial pressure falls because of blood pooling in the legs and splanchnic circulation. Our model suggests that there is also an initial increase in cerebrovascular resistance. This may be due to unloading of baroreceptors in the carotid arteries, aortic arch, and cardiopulmonary circulation during the initial blood pressure decline, causing reflex cardioacceleration and both systemic and cerebral vasoconstriction. However, recent studies in normal and spinal cord-injured subjects suggest that the cerebral circulation is weakly innervated by the sympathetic nervous system. Other work examining the response of spinal cord-

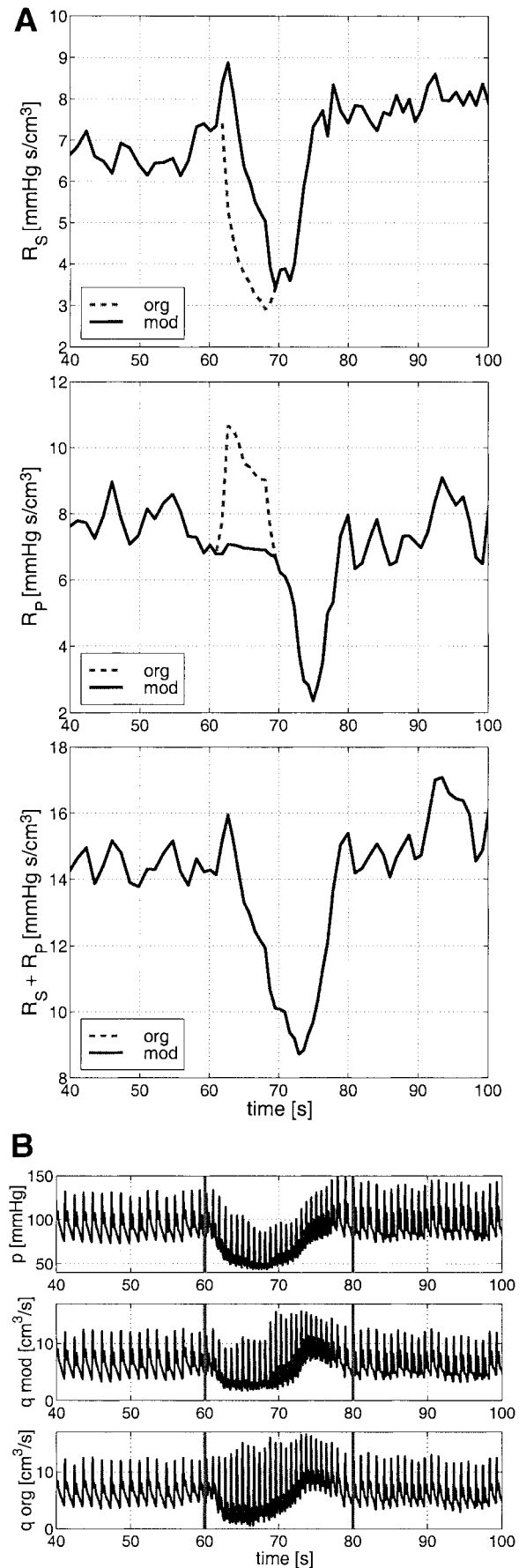


Fig. 11. A: both the modified (solid line) and the original (dashed line) parameters (R_S , R_P , and $R_S + R_P$) without and with the initial increase in cerebrovascular resistance R_P . Note that the total resistance is kept constant by modifying both R_S and R_P . B: finger pressure p (input to the model) and the modified (middle) and original (lower) computed flows q . Without the initial increase in the cerebrovascular resistance R_P , the blood flow pulse does not widen (middle trace in B).

injured patients to head-up tilt has found cerebral blood flow decreased (14, 49) or remain unchanged (23, 24) during arterial hypotension. Furthermore, direct infusions of norepinephrine in both anesthetized (37) and conscious able-bodied patients (26) have not been shown to affect cerebral blood flow or vascular resistance. Therefore, the initial increase in cerebrovascular resistance we observed may be a passive, rather than baroreflex-mediated, response, due to a greater reduction in cerebral blood flow relative to mean arterial blood pressure during posture change.

When cerebral autoregulation becomes engaged approximately 10 s after the initial fall in pressure, cerebrovascular resistance decreases as expected, to restore cerebral blood flow back to baseline. The initial increase in cerebrovascular resistance may explain the widening of the cerebral blood flow pulse velocity which was observed in the young subjects. Figure 11A shows that if we modify the cerebrovascular resistance to prevent its increase (while keeping the total resistance constant) the blood flow pulse does not widen (see Fig. 11B). In our previous study of elderly subjects (20), flow pulses did not widen during posture change. Although further research is needed, this may now be explained by the absence of the initial cerebral vasoconstriction.

One important limitation of our work is the assumption that the finger pressure can be used as input to the model. The forearm responds to the unloading of baroreceptors with vasoconstriction that may uncouple the central blood pressure from the finger pressure. However, even using the finger pressure in the simple model adopted here we were able to achieve good comparisons between the measured and computed data. If future studies can measure cerebral perfusion pressure more directly, our model should be even more relevant. We agree with the conclusion in the recent work by Quick et al. (31) that even such simple models “can play a vital role in solving aspects of the inverse problem.” [By the inverse problem, it is meant inferring properties of the arterial system from measured pressure and flow. Quick et al. (31) point out that the solution to such inverse problems is not generally unique.] Our main conclusion is that there is a biphasic response to orthostatic hypotension during the transition from sitting to standing. Cerebral vascular resistance increases first, before an autoregulatory decrease in resistance begins to dominate the control.

Perspectives

The lumped parameter model presented in this paper demonstrates a biphasic cerebrovascular response to acute posture change in healthy young subjects. This is characterized by initial peripheral cerebral vasoconstriction (manifested by increased pulsatility), followed by autoregulatory cerebral vasodilation. The unique finding of initial vasoconstriction remains unexplained, but may represent rapidly acting baroreflex control of the cerebral circulation, or passive mechanisms due to greater initial reduction in cerebral blood flow relative to the reduction in mean arterial pressure during standing.

Given its success in reproducing the dynamic changes in cerebral blood flow seen during posture change, this model may be helpful in elucidating mechanisms of abnormal cerebral autoregulation in a variety of pathological conditions. For example, the “paradoxical” increase in pulsatility reported during orthostatic stress in patients with vasovagal syncope (9, 10) might be explained by the early vasoconstriction revealed by our model. Because earlier studies did not examine the dynamics of cerebral blood flow response, they may have failed to recognize a later vasodilation after posture change that reflects normal autoregulation. The model might also be useful in the study of autoregulatory changes with aging, hypertension, and cerebrovascular disease.

The modeling was supported by a Group Infrastructure Grant No. DMS-9631755 from the National Science Foundation. The data collection and analysis was supported by a Joseph Paresky Men's Associates grant from the Hebrew Rehabilitation Center for Aged, a Research Nursing Home Grant #AG04390, and an Alzheimers Disease Research Center Grant #AG05134 from the National Institute on Aging. Dr. Lipsitz holds the Irving and Edyth S. Usen and Family Chair in Geriatric Medicine at the Hebrew Rehabilitation Center for Aged.

REFERENCES

1. **Aaslid R, Lindegaard KF, Sorteberg W, and Nornes H.** Cerebral autoregulation dynamics in humans. *Stroke* 20: 45–52, 1989.
2. **Anliker M, Rockwell RL, and Ogden E.** Nonlinear analysis of flow pulses and shock waves in arteries. *Zeitschr Angew Math Phys* 22: 217–246, 1971.
3. **Bekker A, Wolk S, Turndorf H, Kristol D, and Ritter A.** Computer simulation of cerebrovascular circulation: assessment of intracranial hemodynamics during induction of anesthesia. *J Clin Monit* 12: 433–444, 1996.
4. **Bishop CCR, Powell D, Rutt C, and Browne NL.** Transcranial doppler measurement of middle cerebral artery blood flow velocity: a validation study. *Stroke* 17: 913–915, 1986.
5. **Brass LM, Prohovnik I, Pavlakakis SG, DeVivo DC, Piomelli S, and Mohr JP.** Middle cerebral artery blood velocity and cerebral blood flow in sickle cell disease. *Stroke* 22: 27–30, 1991.
6. **Daffertshofer M, Diehl RR, Ziemis GU, and Hennerici M.** Orthostatic changes of cerebral blood flow velocity in patients with autonomic dysfunction. *J Neurol Sci* 104: 32–38, 1991.
7. **Dahl A, Russell D, Nyberg-Hansen R, Rootwelt K, and Bakke SJ.** Cerebral vasoreactivity in unilateral carotid artery disease. A comparison of blood flow velocity and regional cerebral blood flow measurements. *Stroke* 25: 621–626, 1994.
8. **Davy KP, Seals DR, and Tanaka H.** Augmented cardiopulmonary and integrative sympathetic baroreflexes but attenuated peripheral vasoconstriction with age. *Hypertension* 32: 298–304, 1998.
9. **Diehl RR, Linden D, Chalkiadaki A, Bernd Ringelstein E, and Berlitz P.** Transcranial doppler during neurocardiogenic syncope. *Clin Auton Res* 6: 71–74, 1996.
10. **Diehl RR, Linden D, Chalkiadaki A, and Diehl A.** Cerebrovascular mechanisms in neurocardiogenic syncope with and without postural tachycardia syndrome. *J Auton Nerv Syst* 76: 159–166, 1999.
11. **DuBoulay G, Symon L, Ackerman RH, Dorsch D, Kendall BE, and Shah SH.** The reactivity of the spastic arteries. *Neurology* 5: 37–39, 1973.
12. **Fincham W and Tehrani FT.** On the regulation of cardiac output and cerebral blood flow. *J Biomed Eng* 5: 73–75, 1983.
13. **Gaffie D, Liebaert P, and Quandieu P.** A mathematical modeling of the cerebrovascular system. *Physiologist* 33, Suppl 1: S157–S158, 1990.

14. **Gonzalez F, Chang JY, Banovac K, Messina D, Martinez-Arizona A, and Kelly RE.** Autoregulation of cerebral blood flow in patients with orthostatic hypotension after spinal cord injury. *Paraplegia* 29: 1–7, 1991.
15. **Hillen B.** The variability of the circle of willis: univariate and bivariate analysis. *Acta Morphol* 24: 87–101, 1986.
16. **Huber P and Handa J.** Effects of contrast material, hypercapnia, hyperventilation, hypertonic glucose and papaverine on the diameter of the cerebral arteries. *Invest Radiol* 2: 17–32, 1967.
17. **Kufahl RH and Clark ME.** A circle of Willis simulation using distensible vessels and pulsatile flow. *J Biomech Eng* 107: 112–122, 1985.
18. **Larsen FS, Olsen KS, Hansen BA, Paulson OB, and Knudsen GM.** Transcranial Doppler is valid for determination of the lower limit of cerebral blood flow autoregulation. *Stroke* 25: 1985–1988, 1994.
19. **Lindegaard KF, Lundar T, Wiberg J, Sjobert D, Aaslid R, and Nornes H.** Variations in middle cerebral artery blood flow investigated with noninvasive transcranial blood velocity measurements. *Stroke* 18: 1025–1030, 1987.
20. **Lipsitz LA, Mukai S, Hamner J, Gagnon M, and Babikian V.** Dynamic regulation of middle cerebral artery blood flow velocity in aging and hypertension. *Stroke* 31: 1897–1903, 2000.
21. **Mathworks Inc.** Signal processing toolbox, for use with Matlab. In: *User's Guide Version 5*. Natick, MA: Mathworks, 2000.
22. **Mathworks Inc.** Statistics toolbox, for use with Matlab. In: *User's Guide Version 5*. Natick, MA: Mathworks, 2000.
23. **Nanda RN, Wyper DJ, Harper AM, and Johnson RH.** The effect of hypocapnia and change of blood pressure on cerebral blood flow in men with cervical spinal cord transection. *J Neurol Sci* 30: 129–135, 1974.
24. **Nanda RN and Dan K.** Blood flow velocity changes in carotid and vertebral arteries with stellate ganglion block: measurement by magnetic resonance imaging using a direct bolus tracking method. *Reg Anesth Pain Med* 23: 600–604, 1976.
25. **Newell DW, Aaslid R, Lam A, Mayberg TS, and Winn HR.** Comparison of flow and velocity during dynamic autoregulation testing in humans. *Stroke* 25: 793–797, 1994.
26. **Olesen J.** The effect of intracarotid epinephrine, norepinephrine, and angiotensin on the regional cerebral blood flow in man. *Neurology* 22: 978–987, 1972.
27. **Olufsen MS.** Structured tree outflow condition for blood flow in larger systemic arteries. *Am J Physiol Heart Circ Physiol* 276: H257–H268, 1999.
28. **Olufsen MS, Peskin CS, Kim Y, Pedersen EM, Nadim EM, and Larsen J.** Numerical simulation and experimental validation of blood flow in arteries with structured-tree outflow conditions. *Annal Biomed Eng* 28: 1281–1299, 2000.
29. **Paulson OB, Strandgaard S, and Edvinsson L.** Cerebral autoregulation. *Cerebrovasc Brain Metab Rev* 40: 161–192, 1990.
30. **Perktold K and Rappisch G.** Computer simulation of local blood flow and vessel mechanics in a compliant carotid artery bifurcation model. *J Biomech* 28: 845–856, 1995.
31. **Quick CM, Young WL, and Noordergraaf WL.** Infinite number of solutions to the hemodynamic inverse problem. *Am J Physiol Heart Circ Physiol* 280: H1472–H1479, 2001.
32. **Segers P, Dubois F, DeWachter D, and Verdonck P.** Role and relevancy of a cardiovascular simulator. *J Cardiovasc Eng* 3: 48–56, 1998.
33. **Serrador JM, Picot PA, Rutt BK, Shoemaker JK, and Bondar RL.** MRI measures of middle cerebral artery diameter in conscious humans during simulated orthostasis. *Stroke* 31: 1672–1678, 2000.
34. **Sorteberg W, Lindegaard KF, Rootwelt K, Dahl A, Russell D, Nyberg-Hansen R, and Nornes H.** Blood velocity and regional blood flow in defined cerebral arterial systems. *Acta Neurochir (Wein)* 97: 47–52, 1989.
35. **Stergiopoulos N, Young DF, and Rogge TR.** Computer simulation of arterial flow with applications to arterial and aortic stenosis. *J Biomech* 25: 1477–1488, 1992.
36. **Strandgaard S and Paulson OB.** Cerebral blood flow in untreated and treated hypertension. *Netherlands J Med* 47: 180–184, 1995.
37. **Strebel SP, Kindler C, Bissonnette B, Tschaler G, and Deanovic D.** The impact of systemic vasoconstrictors on the cerebral circulation of anesthetized patients. *Anesthesiology* 89: 67–72, 1998.
38. **Toy SM, Melbin J, and Noordergraaf A.** Reduced models of arterial systems. *IEEE Trans Biomed Eng* 32: 174–176, 1985.
39. **Ursino M.** A mathematical study of human intracranial hydrodynamics. Part 1. The cerebrospinal fluid pulse pressure. *Ann Biomed Eng* 16: 379–401, 1988.
40. **Ursino M.** A mathematical model of overall cerebral blood flow regulation in the rat. *IEEE Trans Biomed Eng* 38: 795–807, 1991.
41. **Ursino M and Di Giammarco P.** A mathematical model of the relationship between cerebral blood volume and intracranial pressure changes: the generation of plateau waves. *Ann Biomed Eng* 19: 15–42, 1991.
42. **Ursino M.** A mathematical model of the carotid-baroreflex control in pulsatile conditions. *Sur Math Ind* 7: 203–220, 1997.
43. **Ursino M, Giullioni M, and Lodi CA.** Relationships among cerebral perfusion pressure, autoregulation, and transcranial doppler waveform: a modeling study. *J Neurosurg* 89: 255–266, 1998.
44. **Ursino M and Lodi CA.** Interaction among autoregulation, CO₂ reactivity, and intracranial pressure: a mathematical model. *Am J Physiol Heart Circ Physiol* 274: H1715–H1728, 1998.
45. **Ursino M.** A mathematical model of the carotid baroregulation in pulsating conditions. *IEEE Trans Biomed Eng* 46: 382–392, 1999.
46. **Viedma A, Jimenez-Ortiz C, and Marco V.** Extended willis circle model to explain clinical observations in periorbital arterial flow. *J Biomech* 30: 265–272, 1997.
47. **Van de Vosse FN, Van Steenhoven AA, Janssen JD, and Reneman RS.** A two-dimensional numerical analysis of unsteady flow in the carotid artery bifurcation. A comparison with three-dimensional in-vitro measurements and the influence of minor stenoses. *Biorheology* 27: 163–189, 1990.
48. **Westerhof N, Bosman F, DeVries CJ, and Noordergraaf A.** Analog studies of the human systemic arterial tree. *J Biomech* 2: 121–143, 1969.
49. **Yamamoto M, Meyer JS, Sakai F, and Jakoby R.** Effect of differential spinal cord transection on human cerebral blood flow. *J Neurol Sci* 47: 395–406, 1980.